

Nonlinear optical catastrophe from a smooth initial beam

A. M. Deykoon

Department of Physics, Worcester Polytechnic Institute, Worcester, Massachusetts 01609-2280

M. S. Soskin

Institute of Physics, National Academy of Science of Ukraine, 46 Prospect Nauki, 252650 Kiev-22, Ukraine

G. A. Swartzlander, Jr.

Department of Physics, Worcester Polytechnic Institute, Worcester, Massachusetts 01609-2280

Received April 7, 1999

We observed an optical cusp diffraction catastrophe with an initially smooth but elongated Gaussian beam with an aspect ratio of 2:1. Nonlinear and linear diffraction regimes account for the near-field elliptical annulus and the far-field spatially complex astroid. © 1999 Optical Society of America
 OCIS codes: 190.4420, 080.1510, 350.6830.

An understanding of self-induced aberrating patterns is important in applications such as laser heating and ablation, laser fusion, and the propagation of intense light beams through guided-wave structures and bulk media (including the atmosphere, liquids, glasses, and crystals). In such materials the refractive index may vary with intensity, resulting in self-deflection of highly asymmetric beams¹ and self-focusing (defocusing)² or counter-self-deflection³ of symmetric beams. For example, in a slightly absorbing liquid a beam with an initially smooth circular cross-sectional intensity profile may form a circular optical shock front or concentric diffraction rings owing to self-defocusing.⁴ Such beam distortions produce unstable or degraded beam characteristics, making it difficult to achieve a highly focused spot. Analytic methods to determine the propagating beam profile do not exist for arbitrary initial conditions, such as when the beam lacks circular symmetry. However, we have discovered a special case in which the beam has an initially smooth elliptical Gaussian profile with an aspect ratio of $\approx 2:1$: The beam develops into a cusp diffraction catastrophe (CDC) over a limited range of powers. Surprisingly, the linear theory of optical caustics accounts for the qualitative and quantitative features of the complex waveforms.

Optical catastrophes are patterns of light that contain optical caustics, i.e., regions of space in which many rays intersect to form bright singularities along a two- or a three-dimensional surface. For example, light passing through an undulated body, droplet, meniscus, or lens can develop caustics. Indeed, such patterns are ubiquitous and can be readily observed (e.g., within a coffee cup, owing to reflections from the polished ceramic surface). The structure of a caustic surface is related to the symmetry of the aberrating body⁵ (which in this Letter is the beam itself). This surface can be formally described in the context

of catastrophe theory by use of the Hamilton–Fermat principle of stationary time to find regions in which light rays touch or intersect.⁶

In our experiment a prism was used to elongate an initially collimated argon laser beam ($\lambda = 514$ nm) with a Gaussian intensity distribution, as shown in Fig. 1. (Such a distortion can also occur in media with inhomogeneous density.) The elliptical beam, with transverse sizes $w_{x,0} = 2.8$ mm and $w_{y,0} = 1.4$ mm, was weakly focused with a lens ($f_{L1} = 200$ mm) into the middle of a vertically aligned nonlinear cell of variable length D , with $D_{\max} = 250$ mm. A movable glass window was used to prevent distortions owing to

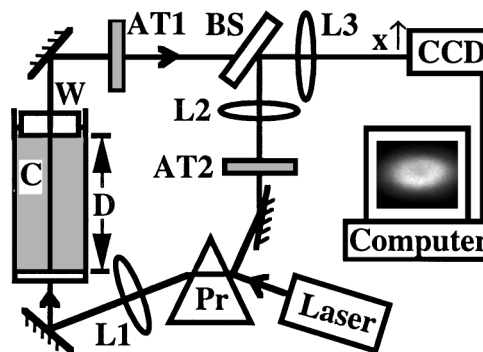


Fig. 1. Schematic diagram of the experimental setup, showing a prism (Pr) that elongates a collimated Gaussian laser beam. A 200-mm focal-length lens (L1) focuses the beam in the center of a nonlinear cell (C) containing slightly absorbing liquid. The cell has a movable output window (W) and a maximum length $D_{\max} = 250$ mm. An attenuator (AT1) and a lens (L3) are used to image the output face of the cell onto a CCD camera (CCD). The images are recorded with a frame grabber and a computer. The optical path comprising L2, AT2, and the beam splitter (BS) is the reference leg of an interferometer.

a meniscus. The cell contained methanol dyed with Nigrosine, and the absorption length and the linear refractive index were $\alpha^{-1} = 360$ mm and $n_0 = 1.33$, respectively. The focusing lens was placed a distance $d = 125$ mm from the input face of the cell, where the beam sizes were $w_x = 1.34$ mm and $w_y = 0.68$ mm. The calculated focused sizes in the medium were $w_x' = 12$ μm and $w_y' = 23$ μm . Note that at the input face the major axis of the ellipse is along the x axis, whereas in the focal plane it is parallel to the y axis (the latter axis is called the conjugate major axis). The optical system included an interferometer for examining the phase of the beam.

As the incident power increased from $P = 0$ to $P \approx 100$ mW the beam at the output face exhibited strong diffraction along the minor axis (y axis), owing to counter-self-deflection,³ and it acquired a complex interference-dominated structure in the center. The complexity of the structure increased and a new pattern exhibiting the characteristics of a CDC emerged as the power was increased to more than 100 mW. In particular, a pronounced astroid-shaped caustic appeared at the output face of the cell when $D = 215$ mm and $P = 156$ mW, as shown in Fig. 2(a). To develop an understanding of the nonlinear propagation dynamics of this phenomenon we varied the propagation distance (see Fig. 3) and recorded the profiles at $D = 103$, 122, 185 mm. Figures 2 and 3 were recorded in the steady-state regime, after ~ 60 s of illumination in the thermal nonlinear medium.

In linear optics a CDC is a generic feature created from an annular elliptical beam with major and minor axes y_e and x_e , respectively, and foci at $f_e = \pm(y_e^2 - x_e^2)^{1/2}$. Such beams have been detected, for example, during the occultation of a star with the planet Mars.⁷ In our experiment this orientation of the ellipse axes ($y_e > x_e$) is the same as that of the conjugate major and minor axes of the beam in the focal region, as shown in Fig. 3(a); hence, the development of the CDC may be traced back to this region. Indeed, at a distance $D = 103$ mm [see Fig. 3(a)] we observed a large beam (~ 580 times the area of the focal spot in the linear case) with the energy concentrated on an annular ellipse. This enlargement is attributed to self-defocusing near the input face of the nonlinear medium. Surprisingly, the characteristics of the observed astroid and the annular ellipse in our nonlinear experiment agree qualitatively with the theoretical correspondence in linear optics, suggesting that propagation over the second half of the cell is dominated by linear diffraction.

Let us now seek a quantitative agreement. According to Huygens's principle, points along an annulus radiate, producing diffracted annular ovals as the beam propagates, as depicted in Fig. 3(b). When the innermost ovals overlap, the beam develops cusp singularities.⁸ With further propagation [see Fig. 3(c)] the interfering wave fronts are bounded by an astroid, i.e., a curve that satisfies $(x/x_a)^{2/3} + (y/y_a)^{2/3} = 1$, with cusps located at $\pm x_a$ and $\pm y_a$. We can understand this evolute from a ray-optics point of view by drawing normals to the tangents of the annular ellipse, as shown in the inset of Fig. 3(c). The astroid is a lo-

cus of points at which many rays coincide, forming an optical caustic containing cusps⁸ at the vertices. Given that many rays cross within the astroid, one can expect significant diffraction and spatial complexity there when coherent light is used. At $D = 250$ mm [see Fig. 2(a)] the image of the astroid is complete (i.e., the annular diffraction ovals are absent). Theoretically an inverse relation exists between the aspect ratios of an annular ellipse and its evolute, the astroid: $y_e/x_e = x_a/y_a$. Thus one can directly compare the annular ellipse in Fig. 3(a) and the astroid in Fig. 2(a). The aspect ratio of the ellipse is found to be $y_e/x_e = 1.31$. For comparison, we plotted the corresponding astroid (with the inverse aspect ratio) on Fig. 2(a) (the value of y_a was fitted to coincide with the caustics). As anticipated, the plot agrees well with the outline of the diffraction envelope and corroborates the assumption that propagation past the focal region is dominated by linear (rather than nonlinear) diffraction.

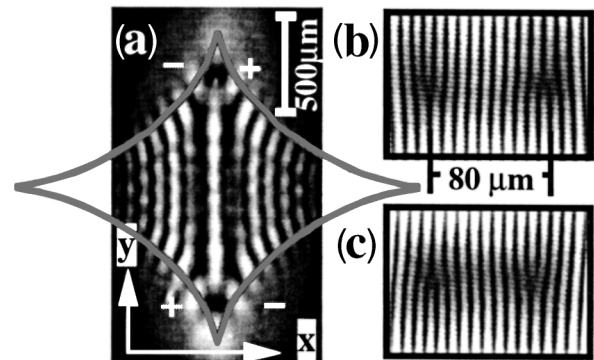


Fig. 2. Nonlinear optical CDC. (a) Intensity profile and (b), (c) magnified interferograms at the cusps at the output face of the nonlinear cell ($D = 215$ mm, $P = 156$ mW). An astroid with an aspect ratio of $1/1.31$ outlines the complex structure in the beam. Optical vortices with a topological charge of ± 1 appear as (a) dark nodes and (b), (c) forks near two of the cusps.

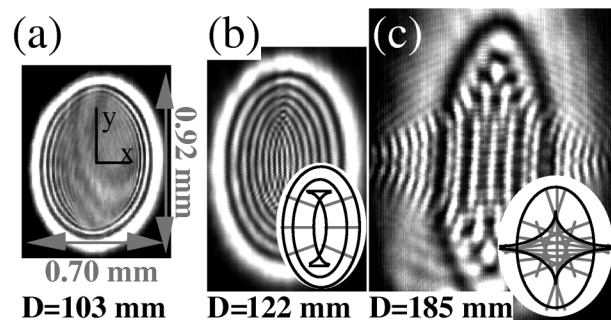


Fig. 3. Propagating beam, showing intensity profiles at the output face of a variable-length nonlinear cell ($P = 156$ mW). (a) Position of minimal beam area at $D = 103$ mm. Aspect ratio, 1.31. (b) Onset of internal interference at $D = 122$ mm. The inset depicts elliptical wave fronts and inward rays of equal length. (c) Nearly complete astroid formation at $D = 185$ mm. The inset depicts rays of equal length that span the ellipse, forming an astroid-shaped evolute.

In contrast to what was observed for CDC's in linear optics, we observed not arrays of stable vortex pairs near the cusps⁶ but rather only a single unstable vortex quadrupole, i.e., a set of four vortices with alternating topological charges, as shown in Fig. 2. This quadrupole appeared when the astroid image was complete ($P = 156$ mW) and vanished when the power was varied by ~ 5 mW. Optical vortices⁹ can form in linear optics when three waves (from coherent non-collinear sources) with roughly the same intensity interfere. However, if the amplitude of one of the waves is significantly greater than the others, then total destructive interference is prohibited, and vortices will not appear. Indeed, an examination of the inset of Fig. 3(c) for an ideal annular ellipse verifies that an arbitrary point within the astroid has exactly three rays passing through it. For the nonlinear case, however, the electric-field distribution in the focal region is not an ideal annular ellipse with a planar wave front [see Fig. 3(a)]; therefore, additional rays may frustrate the formation of vortices. It is evident from Fig. 3(c) that dark nodes resembling closely spaced vortices occur; however, interferometric measurements indicated that these nodes are not vortices [i.e., the interferograms do not resemble Fig. 2(b) or 2(c)]. At lower power, however, we did observe one, two, and three sets of quadrupoles along the perimeter of the beam, owing to nonlinear lensing,¹⁰ for $P = 26$ mW, $P = 34$ mW, and $P = 42$ mW, respectively. Previously, only single quadrupoles were reported.¹¹

In summary, the nonlinear optical cusp diffraction catastrophe is characterized by a two-step process. First, the beam energy is redistributed in the vicinity of the focal plane through nonlinear refraction. We found that the beam developed into an annular ellipse with a significantly enlarged beam area compared with that in the linear case. Second, the beam undergoes quasi-linear propagation beyond this region, resulting in the formation of an astroid under certain conditions. We examined the beam at the output face of the nonlinear cell as power was increased from zero and found that the system exhibited characteristics of an unstable system: first, a deterministic increase in the output intensity (with vortex quadrupoles appearing at the perimeter of the beam), followed by diffractive oscillations across the beam (owing to quasi-one-dimensional counter-self-deflection), and finally

spatial complexity at high powers (with the appearance of the CDC). Thus, in a self-defocusing-type nonlinear system, spatial complexity can develop from a smooth unperturbed initial beam. This effect arises when the beam becomes elongated (e.g., owing to inhomogeneities in the material). Hence we suggest that this instability can be managed in applications involving high-power lasers by control of the aspect ratio of the beam to counter this elongation.

G. A. Swartzlander's e-mail address is grovers@wpi.edu.

References

1. A. E. Kaplan, Pis. Zh. Eksp. Teor. Fiz. **9**, 58 (1969) [JETP Lett. **9**, 33 (1969)]; G. A. Swartzlander, Jr., H. Yin, and A. E. Kaplan, J. Opt. Soc. Am. B **6**, 1317 (1989).
2. S. A. Akhmanov, R. V. Khokhlov, and A. P. Sukharukov, in *Laser Handbook*, F. T. Arecchi, ed. (North-Holland, Amsterdam, 1972).
3. G. A. Swartzlander, Jr., and A. E. Kaplan, J. Opt. Soc. Am. B **5**, 765 (1988).
4. J. P. Gordon, R. C. Leite, R. S. Moore, S. P. S. Porto, and J. R. Whinnery, J. Appl. Phys. **36**, 3 (1965); J. R. Whinnery, D. T. Miller, and F. Dabby, IEEE J. Quantum Electron. **QE-3**, 382 (1968).
5. R. Thom, *Stabilitestructurelle et Morphogenes* (Benjamin, Reading, Mass., 1972) [updated English translation, *Structural Stability and Morphogenesis* (Benjamin, Reading, Mass., 1975)].
6. M. V. Berry and C. Upstill, in *Progress in Optics XVIII*, E. Wolf, ed. (North-Holland, Amsterdam, 1980), p. 257.
7. J. L. Elliot, R. G. French, E. Dunham, P. J. Gierasch, J. Veverka, C. Church, and C. Sagan, Astrophys. J. **217**, 661 (1977).
8. V. I. Arnol'd, *Catastrophe Theory*, 3rd ed. (Springer-Verlag, Berlin, 1992), Chap. 8.
9. J. F. Nye and M. V. Berry, Proc. R. Soc. London Ser. A **336**, 165 (1974).
10. L. V. Kreminskaya, M. S. Soskin, and A. I. Khizhnyak, Opt. Commun. **145**, 337 (1997).
11. T. Ackermann, E. Kriege, and W. Lange, Opt. Commun. **115**, 339 (1995); A. V. Il'yankov, A. I. Khizhnyak, L. V. Kreminskaya, M. S. Soskin, and M. V. Vasnetsov, Appl. Phys. B **62**, 465 (1996); A. V. Il'yankov, L. V. Kreminskaya, M. S. Soskin, and M. V. Vasnetsov, Int. J. Nonlinear Opt. Phys. Mater. **6**, 169 (1997).